Influence of diagenesis on the stable isotopic composition of biogenic carbonates from the Gulf of Tehuantepec oxygen minimum zone

Cécile Blanchet, S Kasten, Laurence Vidal, S. W. Poulton, R Ganeshram, Nicolas Thouveny

Influence of diagenesis on the stable isotopic composition of biogenic carbonates from the Gulf of Tehuantepec oxygen minimum zone

C. L. Blanchet

Department of Geophysics, University of Bremen, Postfach 330440, D-28334 Bremen, Germany

Now at Paleoceanography Group, GEOMAR, Helmholtz Centre for Ocean Research Kiel, East Shore Campus, Wischhofstraße 1-3, D-24148 Kiel, Germany (cblanchet@geomar.de)

S. Kasten

Marine Geochemistry, Alfred Wegener Institute for Polar and Marine Research, Am Handelshafen 12, D-27570 Bremerhaven, Germany

L. Vidal

CEREGE, Aix-Marseille University, CNRS, IRD, CdF, Europôle Méditerranéen de l'Arbois, Avenue Louis Philibert BP 80, F-13545 Aix en Provence CEDEX 04, France

S. W. Poulton

School of Civil Engineering and Geosciences, Newcastle University, Newcastle upon Tyne NE1 7RU, UK

R. Ganeshram

John Murray Laboratories, The King's Buildings, West Mains Road, Edinburgh EH9 3JW, UK

N. Thouveny

CEREGE, Aix-Marseille University, CNRS, IRD, CdF, Europôle Méditerranéen de l'Arbois, Avenue Louis Philibert BP 80, F-13545 Aix en Provence CEDEX 04, France

[1] In order to evaluate the influence of diagenetic and post-sampling processes on the stable oxygen and carbon isotope compositions of biogenic carbonates, we conducted a multiproxy study of organic-rich sediments from the eastern Pacific oxygen minimum zone. Core MD02-2520, which was retrieved from the Gulf of Tehuantepec (Mexico), has seasonal laminations and covers the last 40 kyr. Together with the presence of gypsum crystals and inorganic calcite aggregates, the occurrence of large excursions in the stable oxygen and carbon isotope records of both planktonic and benthic foraminifera (as large as +3‰ in $\delta^{18}O$ and −5‰ in $\delta^{13}C$) point to significant secondary transformations. Storage-related gypsum precipitation was ruled out since it implies sulfide reoxidation by oxygen that triggers biogenic calcite dissolution, which proved to be of minor importance here. Instead, precipitation of authigenic calcite during early diagenesis appears to be the most likely process responsible for the observed isotopic excursions. The $\delta^{13}C$ composition for inorganic calcite aggregates (−5 to −7‰) suggests a major contribution from anaerobic oxidation of organic matter. The $\delta^{34}S$ composition for gypsum crystals (−10 to +15‰) suggests a major contribution from anaerobic reoxidation of authigenic sulfides, potentially involving reactions with metal oxides and sulfur disproportionation. A minor part of the gypsum might possibly have formed as a result of local pore water salinity increases induced by gas hydrate formation.

1. Introduction

[2] Paleoclimatic reconstructions often rely on the information provided by the biogenic carbonate fraction of marine sediments. Indeed, the composition of stable oxygen isotopes in fossil foraminifera, which was initially related to seawater temperature [*Emiliani*, 1955], is widely used to monitor past variations in water column chemical and physical properties [*Duplessy et al.*, 1991]. Combining stable oxygen and carbon isotopic analyses ($\delta^{18}O$ and $\delta^{13}C$) for foraminifer species living at different water depths allows reconstruction of temporal changes in temperature, salinity and ventilation within various water masses [*Spero et al.*, 2003]. However, the primary (oceanographic) record can be overprinted by secondary processes such as: i) the precipitation of inorganic calcite on the tests [*Reuning et al.*, 2005], and ii) the dissolution of specific calcite layers from the tests [*Berger and Killingley*, 1977]. Such processes may occur either *in situ* during early diagenesis or *ex situ* during sediment storage.

[3] Prolonged exposure of marine sediments to oxygen during storage generally leads to oxidation of the reduced sulfur species to dissolved sulfate (SO_4^{2-}) or elemental sulfur and can also induce the precipitation of solid sulfate minerals such as gypsum ($CaSO_4 \cdot 2H_2O$) [*Schnitker et al.*, 1980; *Self-Trail and Seefelt*, 2005; *Dunkley-Jones and Brown*, 2007]. Together with oxidation of organic matter, these sulfide oxidation reactions tend to lower the pore water pH and trigger the dissolution of biogenic carbonates [*Schnitker et al.*, 1980; *Sperling et al.*, 2002; *Self-Trail and Seefelt*, 2005].

[4] During diagenesis, both precipitation of inorganic calcite and dissolution of biogenic carbonates can occur [e.g., *Reimers et al.*, 1996; *Jahnke et al.*, 1997]. Calcite dissolution is generally induced by aerobic mineralization of organic matter [*Jahnke et al.*, 1997; *Pfeifer et al.*, 2002]. Precipitation of authigenic calcite as coatings on foraminifera or as aggregates may be associated with organic remineralization reactions involving iron oxides and/or sulfate reduction reactions, releasing carbonate ions into the pore water [*Reimers et al.*, 1996]. Oversaturation of pore waters with respect to calcite tends to occur close to the so-called sulfate-methane transition (SMT), where sulfate reduction driven by methane leads to an increase in alkalinity [e.g., *Peckmann et al.*, 2001; *Treude et al.*, 2005; *Nöthen and Kasten*, 2011]. Precipitation of authigenic barium sulfate (barite) has also been demonstrated to occur around the SMT [e.g., *Torres et al.*, 1996; *Dickens*, 2001; *Riedinger et al.*, 2006], which can often be distinguished from biogenic barite formed in the water column by stable sulfur isotope signatures [*Torres et al.*, 1996; *Paytan et al.*, 2002]. Gypsum crystals have also been identified in freshly recovered sediments, which indicates that gypsum can form *in situ* [*Siesser and Rogers*, 1976; *Briskin and Schreiber*, 1978; *Hoareau et al.*, 2011]. Calculations of gypsum saturation in several sediment cores drilled in the frame of the Ocean Drilling Program and the Integrated Ocean Drilling Program (ODP/IODP) revealed that gypsum formation in marine sediments is related either to the presence of evaporitic brines or volcanogenic material [*Hoareau et al.*, 2011]. However, gypsum crystals have also been observed in sediments barren of evaporitic or volcanogenic material [*Siesser and Rogers*, 1976; *Briskin and Schreiber*, 1978; *Muza and Sherwood*, 1983]. In the study of *Siesser and Rogers* [1976], gypsum crystals were thought to have grown in organic-rich suboxic sediments, where low pore water pH induced by high rates of iron sulfide precipitation led to dissolution of the foraminifera. The calcium ions released by this process may then have reacted with residual pore water sulfate ions
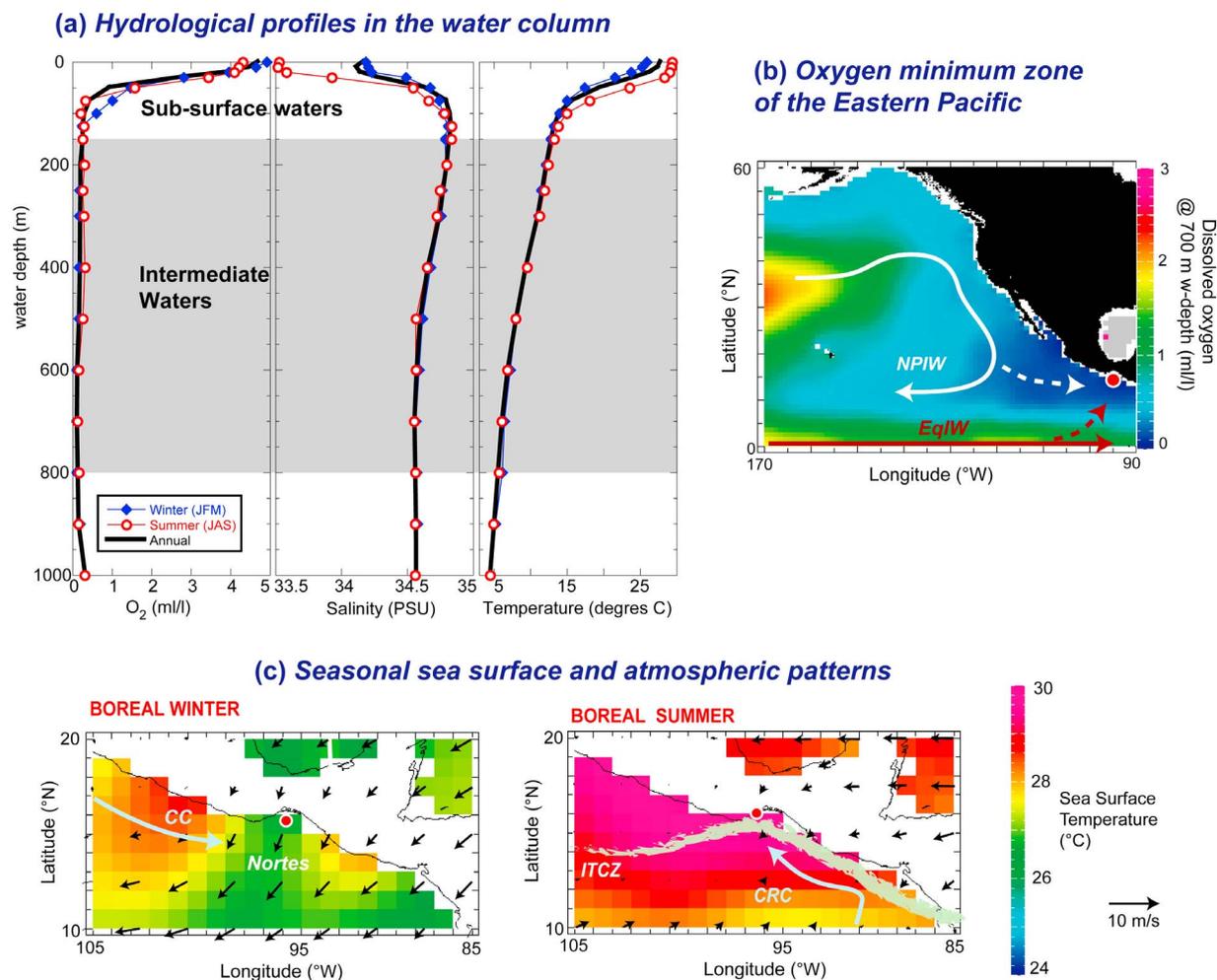
(a) *Hydrological profiles in the water column*

(b) *Oxygen minimum zone of the Eastern Pacific*

(c) *Seasonal sea surface and atmospheric patterns*

Figure 1. Oceanography and climatic regimes in the Gulf of Tehuantepec. (a) Profiles of dissolved oxygen, salinity and temperature at 15.5°N 95.5°W (winter: filled blue diamonds; summer: open red circles; annual average: black line) [*Conkright et al.*, 2002]. (b) Spatial extension of the Oxygen Minimum Zone of the eastern Pacific: Dissolved O_2 content at 700 m water-depth [*Conkright et al.*, 2002; *Schlitzer*, 2008]. Intermediate water masses: North Pacific Intermediate Water (NPIW) and Equatorial Intermediate Water (EqIW). (c) Sea surface temperatures and wind fields during boreal summer and winter [*Conkright et al.*, 2002; *Kalnay et al.*, 1996]. Surface currents: California Current (CC) and Costa Rica Current (CRC), Intertropical Convergence Zone (ITCZ).

to form gypsum, although such a process has not been unequivocally demonstrated. Indeed, *Reimers et al.* [1996] showed that the pore water pH of organic-rich sediments is generally higher than 7, due to the dominance of sulfate reduction over iron sulfide precipitation. Therefore, the biogeochemical mechanism leading to formation of authigenic gypsum in marine sediments (barren of evaporitic or volcanogenic material) are still largely unresolved, and the impact of such processes on the stable isotope composition of foraminifera is unknown.

[5] Here, we investigate a sediment core from the Gulf of Tehuantepec (Pacific margin off southern Mexico) that contains high levels of organic carbon and has mm-scale laminations. These sediments are typical of surface sediments from the eastern Pacific oxygen minimum zone (OMZ) [*van Geen et al.*, 2003], which is the oxygen-depleted water mass bathing the Californian and Mexican margins (Figure 1) [*Paulmier and Ruiz-Pino*, 2009]. In the sediments from the Gulf of Tehuantepec, mm-scale gypsum crystals and inorganic calcite aggregates were identified, and large excursions were observed in the carbon and oxygen isotope signature of various

foraminifera species. In order to determine the origin of the gypsum and calcite aggregates, we measured their sulfur, carbon and oxygen isotope composition, with the aim of determining the cause of the observed isotopic excursions and their potential link to gypsum and inorganic calcite formation.

2. Regional and Oceanographic Settings

[6] The Gulf of Tehuantepec is located in the southern part of the Pacific coast off Mexico. Based on the physical and chemical characteristics of the water column, two water masses can be distinguished (Figure 1a): the sub-surface waters (0 to 150 m water-depth) and the intermediate waters (150 to 800 m water-depth). In the summer, the surface waters are warm ($\sim$28°C) and have a low salinity ($\sim$33.5 PSU) because of large precipitation and river runoff related to the activity of the inter-tropical convergence zone (ITCZ) and the north-ward inflow of the Costa Rica Current (Figure 1c) [*Molina-Cruz and Martinez-Lopez*, 1994]. In winter, the surface waters are cooler (25°C) and more saline (>34 PSU), the thermocline is shallow (50 m) and the water column is poorly stratified. These characteristics are due to: i) coastal upwelling induced by strong southward winds blowing on the Tehuantepec Isthmus, ii) very little precipitation, due to the southward migration of the ITCZ and iii) the southward inflow of the California Current [*Färber-Lorda et al.*, 2004].

[7] Intermediate waters in the Gulf of Tehuantepec have low contents of dissolved oxygen (<0.5 ml/l), low temperatures (<14°C) and high salinity (>34.5 PSU) (Figure 1a). This permanent oxygen depletion extends from 10 to 50°N along the American margin (Figure 1b) [*Paulmier and Ruiz-Pino*, 2009]. Although still unclear, the causes of the oxygen depletion within the OMZ are believed to be related to organic matter degradation in the water column due to high levels of primary productivity in surface waters and to lateral advection of oxygen-depleted water [*Paulmier and Ruiz-Pino*, 2009]. The Gulf of Tehuantepec lies at the boundary between the North Pacific Intermediate Water (NPIW) and the Equatorial Intermediate Water (EqIW) (Figure 1), which is a mixture of Antarctic Intermediate Water (AAIW) and upwelled Pacific Deep Water (PDW) [*Lacan and Jeandel*, 2001]. Previous studies in the Gulf of Tehuantepec [*Hendy and Pedersen*, 2006] and along the Baja California peninsula [*Basak et al.*, 2010; *Cartapanis et al.*, 2011] showed that chemical properties of

intermediate waters in the OMZ reflected a balancing influence from northern (NPIW) and southern (EqIW) sources during the past 40 kyr.

3. Material and Methods

3.1. Core Description

[8] Sediment core MD02-2520 was retrieved at 712 m water-depth on the slope of the continental margin off Tehuantepec (15.4°N, 95.2°W) (Figure 1). The core was collected using a Calypso piston corer on board the R/V Marion Dufresne in June 2002 during the International Marine Past Global Change Study (IMAGES) Campaign MD126 Marges Ouest Nord Américaines (MONA) [*Beaufort et al.*, 2002]. The 37 m-long sediment core shows an alternation of dark-colored and light-colored silty-clays deposited as sub-mm laminations. The dark-colored layers are mainly composed of terrigenous and organic material (of olive-gray color) and the light-colored layers contain marine biogenic detritus (foraminifera, diatoms). Detailed counting of the laminations and age determinations (see section 3.3) reveal that a couplet of light- and dark-colored laminae correspond to an annual deposit [*Blanchet*, 2006]. Several cm-thick dark- or light-colored intervals show traces of bioturbation and therefore no laminations. Some silty-sand intervals are documented between 3 and 12 m core depth. Partial sediment expansions during core recovery suggest the *in situ* presence of gas hydrates in the sedimentary column at 16–16.5 m, 29 m, 32.2 m, and 34.7 m core depth.

3.2. Analytical Methods

3.2.1. Stable Isotopes of Oxygen and Carbon

[9] Four species of fossil foraminifera were picked from core MD02-2520:

[10] 1. *Globigerinoides ruber* and *Neogloboquadrina dutertrei* are two symbiotic planktonic foraminifera, with *G. ruber* living in the subsurface (upper 50 m water-depth) in summer, and *N. dutertrei* living around the thermocline ($\sim$50 m water-depth) in winter [*Thunell et al.*, 1983; *Spero et al.*, 2003].

[11] 2. *Uvigerina peregrina* and *Brizalina sp.* are two shallow infaunal benthic foraminifera living between 2 and 7 cm sediment depth [*McCorkle et al.*, 1997].

[12] Centimeter-thick slices of sediment, collected every five or ten cm, were sieved under water and split into two size fractions: 63–250 μm and

Table 1. Age Control in Core MD02-2520[a]

Species	Depth (cm)	¹⁴C Age (yr BP)	Reserv.-Corr. ¹⁴C Age (yr BP)	95.4% (2σ) Cal. Age Range (cal. BP)	Calendar Age (cal. BP)
G. ruber	173	2030 ± 70	1574	1255–1615	1435 ± 180
G. ruber/G. bulloides	343	3370 ± 50	2914	2827–3227	3030 ± 200
G. ruber	393	4020 ± 50	3564	3622–4023	3820 ± 200
G. ruber	553	5080 ± 60	4624	4994–5448	5220 ± 230
G. ruber	833	7870 ± 90	7414	7962–8367	8165 ± 200
G. ruber	1271	13800 ± 130	13344	15203–16197	15970 ± 490
G. bulloides	1271	13970 ± 130	13514	15409–16441	
N. dutertrei	1271	13830 ± 90	13374	15300–16180	
G. bulloides	1471	15530 ± 150	15074	17732–18694	18200 ± 450
N. dutertrei	1471	15470 ± 100	15014	17782–18601	
G. bulloides	1865	19330 ± 140	18724	22048–22587	22300 ± 270
N. dutertrei	2226	21800 ± 160	21344	25248*	25250*
G. ruber/G. bulloides	2295	22350 ± 130	21894	25858*	25990*
N. dutertrei	2295	22590 ± 120	22134	26124*	

[a]¹⁴C ages measured on *G. ruber*, *G. bulloides* and *N. dutertrei* at various core depths. All ages were corrected from a reservoir age of 456 yrs [*Berger et al.*, 1966]. The ages younger than 25 ¹⁴C ka were calibrated using the curve established by *Hughen et al.* [2004] and the older ones (indicated by an asterisk) using the equation established by *Bard et al.* [2004].

>250 μm. From the larger size fraction, four to thirty adult specimens were hand-picked under the binocular to obtain samples weighing between 50 and 90 μg. Between 8 and 37 m, mm-scale tabular gypsum crystals were identified in some of the samples.

[13] The oxygen and carbon isotope compositions of the foraminifera were analyzed at CEREGE (see the auxiliary material).[1] The samples were reacted in orthophosphoric acid (H_3PO_4) at 70°C in a carbonate device (Karbo-Kiel III) and the evolved CO_2 was analyzed by a Thermo-Finnigan Delta-advantage mass spectrometer. Stable isotope ratios are reported in ‰ relative to the V-PBD standard, where

$$\delta^{18}O = \left[\frac{\left(^{18}O/^{16}O\right)_{sample}}{\left(^{18}O/^{16}O\right)_{standard}} - 1 \right] * 1000$$

$$\delta^{13}C = \left[\frac{\left(^{13}C/^{12}C\right)_{sample}}{\left(^{13}C/^{12}C\right)_{standard}} - 1 \right] * 1000.$$

Analytical precisions of 0.05‰ for $\delta^{18}O$ and 0.03‰ for $\delta^{13}C$ were computed from repeat analyses of a limestone NBS-19 standard. We performed 300 analyses and 25 replicates on outliers, which were averaged when values did not differ by more than 0.2‰, and otherwise rejected. The resolution of our record varies with depth in the core due to a complete lack of foraminifera at certain intervals.

3.2.2. Stable Isotopes of Sulfur

[14] Sulfur isotope compositions were analyzed on the gypsum crystals at Iso-Analytical Ltd., UK (see auxiliary material). The crystals were cleaned and carefully ground. Then 0.4 ± 0.04 mg of gypsum powder was mixed with vanadium pentoxide to reach a final weight of about 4 mg. The samples were combusted in the presence of oxygen (at 1080°C) to produce SO_2, N_2, CO_2, and water. After removal of the water (using a Nafion[TM] membrane), SO_2 was isolated from N_2 and CO_2 using a gas chromatograph column, and then analyzed by an elemental analyzer-isotope ratio mass spectrometer (EA-IRMS). Stable isotope ratios are reported in ‰ relative to the V-CDT standard, where

$$\delta^{34}S = \left[\frac{\left(^{34}S/^{32}S\right)_{sample}}{\left(^{34}S/^{32}S\right)_{standard}} - 1 \right] * 1000.$$

[15] Analytical precision better than 0.09‰ and reproducibility of 0.05‰ were obtained by replicate measurements of in-house ($\delta^{34}S_{V-CDT} = +20.74$‰) and international (IAEA-SO-5, $\delta^{34}S_{V-CDT} = +0.50$‰) barium sulfate standards.

3.2.3. Scanning Electron Microscopy

[16] Several specimens of foraminifera and a number of gypsum crystals were imaged using a variable pressure Scanning Electron Microscope (Hitachi 3000N) with a tungsten electron source at CEREGE. The magnification ranged from 5× to 300× with a resolution of 3 nm at 25 kV.
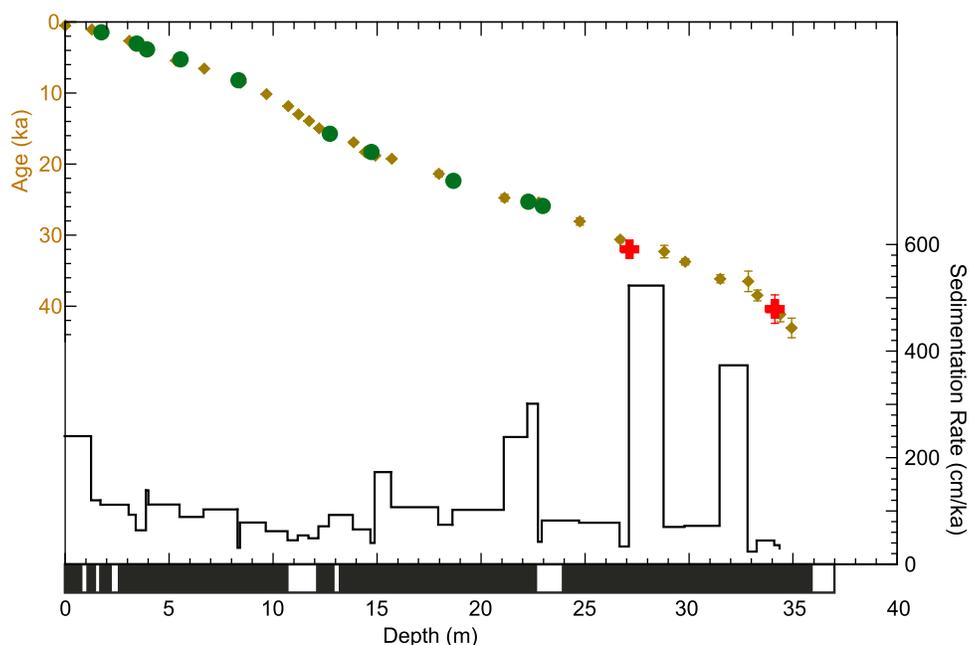
Figure 2. Age model for core MD02-2520. Upper plot: dated points. Green dots: calibrated AMS-^{14}C ages of planktonic foraminifera (error bars comprised in the dot); yellow diamonds: calibrated AMS-^{14}C ages of bulk organic matter [*Pichevin et al.*, 2010]; Red crosses: paleomagnetic excursions (Mono Lake, 32 ka and Laschamp, 40.4 ka). Lower plot: sedimentation rates calculated between each dated point. Black rectangles in the lowest panel show the laminated intervals.

3.2.4. X-Ray Diffraction

[17] Mineralogical determinations were realized in the X-Ray Group at the CEREGE, using a Phillips powder X-Ray diffractometer Philips theta-2 theha (PW1050/81goniometer and PW3710 microprocessor-based diffractometer control unit) equipped with a cobalt anticathode. Data were acquired between 3° and 80° every 0.05°.

3.3. Age Determination

[18] The sediment age was determined using accelerator mass spectrometry (AMS) ^{14}C dating of planktonic foraminifera (*G. ruber*, *Globigerina bulloides* and *N. dutertrei*) at the Tandetron accelerator mass spectrometer in Gif-sur-Yvette (France) (Table 1 and Figure 2). All ages were corrected for a constant surface reservoir age of 456 years, obtained on a shell of *Turritella leverostoma vgl.* in Baya de Guatulco (16°N, 96°W) [*Berger et al.*, 1966]. Ages younger than 25 ka were adjusted on the calibration curve Marine04 [*Hughen et al.*, 2004], using the Calib 5.0 software [*Stuiver et al.*, 2005]. Older ages were corrected using the equation from *Bard et al.* [2004], tied to GISP2. Potential mismatches between the ages given by the surface-dwelling *G. ruber* and *G. bulloides* and the

thermocline-dwelling *N. dutertrei* were assessed by measuring replicate ^{14}C ages for mono-specific samples at various depths (at 12.71, 14.71 and 22.95 m). The mono-specific replicates show no significant age differences, and thus they were averaged to produce a mean age for each sediment depth (Table 1).

[19] Palaeomagnetic measurements performed throughout the core complete the chronological data set [*Blanchet*, 2006]. Large amplitude deviations of the inclination and declination at ~27 m and ~34 m suggest the occurrence of paleomagnetic excursions that were attributed to the Mono Lake and the Laschamp excursions, respectively dated at 32 ka [*Benson et al.*, 2003] and at 40.4 ± 2 ka [*Guillou et al.*, 2004].

[20] Our age determination is in good agreement with that of *Pichevin et al.* [2010], who performed AMS ^{14}C dating on bulk organic matter for core MD02-2520. These ages were calibrated following a similar procedure to the one used for the ages of foraminifera and were also used for the age model. The depth-to-age transformation was achieved using linear interpolations between dated layers. Sedimentation rates vary between 30 and 520 cm.ka^{-1} around a mean of 100 cm.ka^{-1}, with highest

sedimentation rates in the upper meter and between 20 and 35 m (Figure 2).

4. Results

4.1. Quantity of Biogenic Carbonate and Gypsum

[21] The number of foraminifera picked for isotopic analysis provides a semi-quantitative evaluation of the amount of biogenic carbonate in the sediments (Figure 3). A decreasing trend in foraminifer content toward the bottom of the core is observed, and gypsum crystals were identified between 8 and 37 m (Figures 3c, 3d, 3f, and 6). Particularly low amounts of foraminifera (with samples sometimes completely barren of foraminifera) were observed between 15 and 18 m, between 20 and 22 m and at the bottom of the core. Many samples throughout the core were characterized by the presence of planktonic foraminifera and the absence of benthic foraminifera (e.g., at ∼19 m). In order to increase the resolution of the stable isotope records, a second batch of samples was processed 10 months after the first batch, with the first batch being processed between 9 and 19 months after core recovery (Figures 3a and 3b). The characteristics of samples from the second batch were very similar to the first batch. In particular, no increase in gypsum was observed between batches, and the number and assemblage of foraminifera remained constant. It should be noted however that samples were not processed immediately following core recovery, and thus we cannot assess the presence of primary gypsum. The total organic carbon (TOC) content (Figure 3e) ranged from 2 to 7 % with most values being around 5 %, and no obvious down-core trend was observed. TOC content also shows no consistent relationship with the amount of foraminifera or the presence of gypsum (Figure 3).

4.2. Isotopic Composition of Biogenic Carbonates

[22] The $\delta^{18}O$ composition for foraminifera collected at the core-top was compared to the predicted carbonate $\delta^{18}O$ composition (Table 2 and Figure 4). These values were obtained using paleotemperature equations established on core-top and cultured foraminifera [Shackleton, 1974; Bemis et al., 1998]. The measured and calculated isotopic compositions agree to within 0.15‰.

[23] The $\delta^{18}O$ records for planktonic and benthic foraminifera have a similar long-term trend

(Figures 4a and 4b). From high values recorded in the 33–15 m interval, the $\delta^{18}O$ gradually decreases between 15 and 10 m (by ∼1.5‰) to reach lower values in the top 10 m. The $\delta^{18}O$ values for G. ruber are lower by ∼2‰ relative to N. dutertrei and this difference is near constant along the core. In the 33–15 m interval, the $\delta^{18}O$ for G. ruber and N. dutertrei varies around values of −1 and 1‰ respectively, and gradually decreases until a depth of 10 m, where values are ∼−2.5 and ∼−0.5 ‰ respectively (Figure 4a). The $\delta^{18}O$ records for both planktonic species are noisy (particularly in the top 15 m) and exhibit large positive excursions: at 27 m (reaching 1.4 and 2.2‰ for G. ruber and N. dutertrei, respectively), at 14.3 m (reaching 2‰ for N. dutertrei) and at 11 m (reaching 0.4 and 1.4‰ for G. ruber and N. dutertrei, respectively). The $\delta^{18}O$ values for the benthic foraminifera species are higher than those for the planktonic foraminifera species. The $\delta^{18}O$ values for Brizalina sp. are slightly lower than those for U. peregrina in the 33–15 m interval (∼3.5 and ∼4‰, respectively) and reach similar values in the top 10 m (∼2.5‰), after a steady decrease between 15 and 10 m (Figure 4b).

[24] All $\delta^{13}C$ profiles exhibit considerable variability, especially in the top 15 m for the planktonic records (Figures 4c and 4d). Values for the two planktonic species vary around 1.5‰ (Figure 4c), with large negative excursions at 27 m (reaching −2.8‰), at 11 m (reaching −2.5 and −0.8‰ for G. ruber and N. dutertrei, respectively) and at 3.5 m (reaching −1.5‰). The $\delta^{13}C$ for Brizalina sp. and U. peregrina varies around −1.3‰ (Figure 4d), with negative excursions at 13 m (reaching −2‰ for Brizalina sp.), at 11.3 m (reaching −1.5‰ for U. peregrina), at 9.7 m (reaching −3.2 and −2‰ for Brizalina sp. and U. peregrina, respectively) and at 3.5 m (reaching −2.7 and −3.7‰ for Brizalina sp. and U. peregrina, respectively).

4.3. Isotopic Composition of Gypsum Crystals

[25] Sulfur isotope compositions were measured on gypsum crystals that were collected between 8 and 34 m core depth (Figures 4e and 4f). The $\delta^{34}S$ values range from −10 to 15‰, with values becoming heavier (from −6 to 4‰) between 34 and 16 m, followed by an abrupt drop to −2‰ and an increase to +14‰ at 15 m. The next point at 12 m reaches the lowest value (−10‰) and the value at the top of the sequence increases to ∼+11‰.
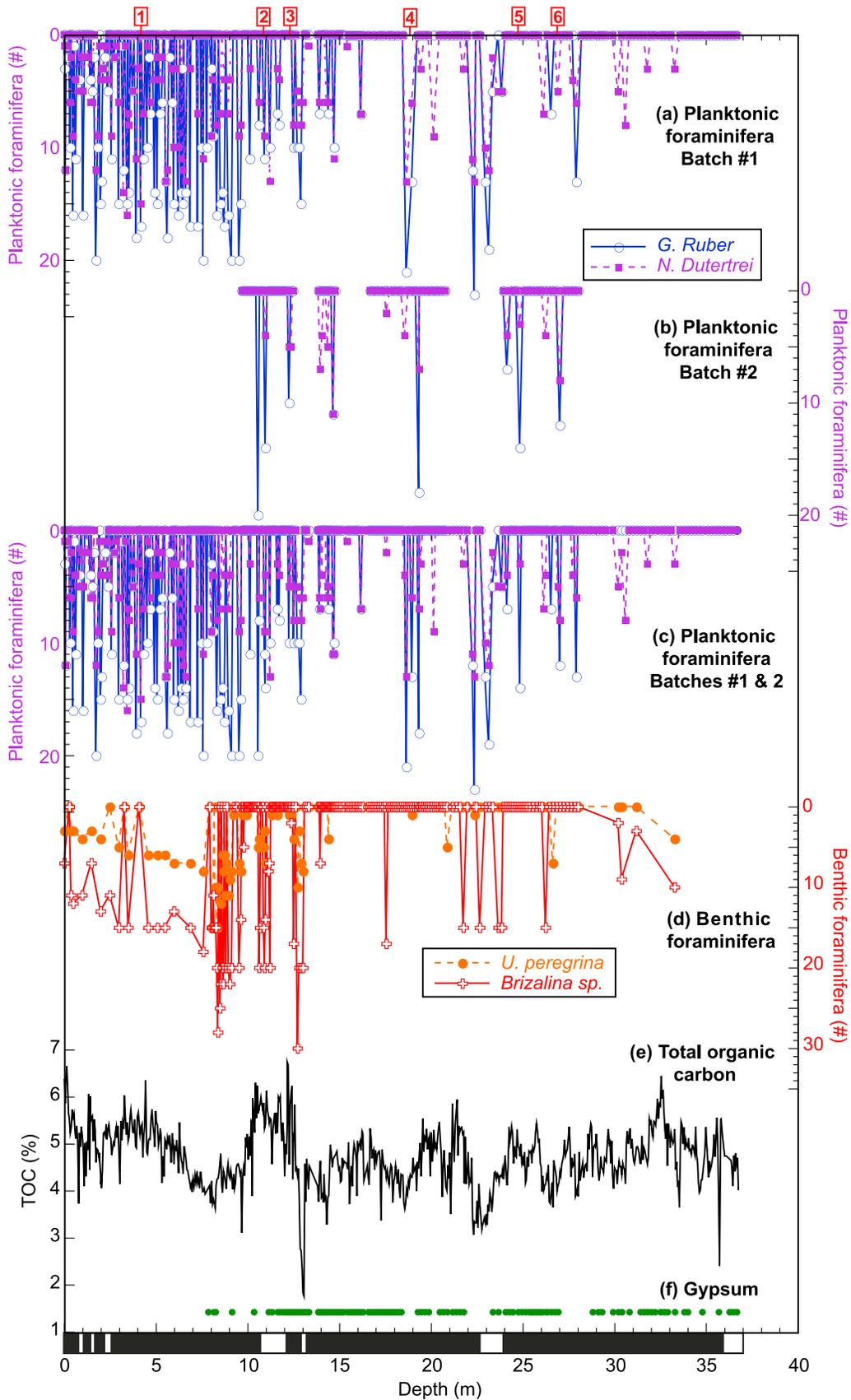
Figure 3

Table 2. Comparison of Measured $\delta^{18}O$ for Core-Top Foraminifera and Inorganic Calcite to the Expected Isotopic Composition of Calcite[a]

	$\delta^{18}O$ Measured (‰ VPDB)	δ_w (‰ VSMOW)	Water Temperature (°C)	δ_c (‰ VPDB)	$\Delta\delta$ (‰ VPDB)	Paleotemp. Equation
Core-Top Foraminifera						
G. ruber	−2.89	0.23	29.33	−3.04	0.15	[1]
N. dutertrei	−0.50	0.17	17.39	−0.62	0.12	[1]
Brizalina sp.	2.57	0.12	6.20	2.52	0.05	[2]
U. peregrina	2.62	0.12	6.20	2.52	0.09	[2]
Inorganic Calcite Formed in Situ						
Holocene	2.14	0.12	6.20	2.34	0.20	[3]
Glacial	4.26	1.12	4.20	3.88	−0.38	[3]

[a]According to paleotemperature equations established by *Bemis et al.* [1998] for planktonic foraminifera [1], *Shackleton* [1974] for benthic foraminifera [2] and *Kim and O'Neil* [1997] for inorganic calcite [3]. For core-top foraminifera, we used seawater $\delta^{18}O$ compositions (δ_w) from the NASA-GISS online database (http://www.giss.nasa.gov/) as given in the work of *Benway and Mix* [2004] and temperatures from *Conkright et al.* [2002] (summer surface temperature for *G. ruber*, winter temperature at 50 m water-depth for *N. dutertrei* and mean annual temperature at 700 m water-depth for the benthic foraminifera, see Figure 1). For the inorganic calcite formed *in situ*, we derived pore-water temperature and δ_w from the bottom-water data for the Holocene. For the Glacial, we adjusted these values to match the measured $\delta^{18}O$ composition of glacial benthic foraminifera (i.e., −2°C and +1‰ respectively, as stated in section 5.1). δ_c is the calculated isotopic composition and $\Delta\delta$ is the difference between the measured and calculated $\delta^{18}O$.

4.4. Isotopic Composition of Inorganic Calcite Aggregates

[26] Oxygen and carbon isotope compositions were analyzed on mm-scale aggregates collected at 5.95 and 25.01 m (Figure 5 and Table 2). The aggregates consist of calcite and magnesian-calcite, with minor contents of quartz, feldspar, pyrite and clays, as determined using X-ray powder diffraction spectra obtained at CEREGE (Figure 6). The $\delta^{18}O$ values range from 2.14 to 4.26‰ and the $\delta^{13}C$ values range from −5.88 to −6.60‰ (Table 2).

4.5. Scanning Electron Microscopy

[27] Images of foraminifera and gypsum crystals are shown in Figure 6. Samples #1 (4.18 m), #4 (18.96 m) and #5 (24.84 m) have foraminifera that are well preserved, as suggested by the absence of filled or connected pores, and these samples do not display isotopic excursions. Sample #5 contains gypsum and carbonate aggregates together with a *G. ruber* specimen that still has thin calcite spines, indicating a particularly good preservation state. Samples #2 (10.92 m), #3 (12.91 m) and #6 (26.54 m) have foraminifera that are affected by both dissolution and re-crystallization processes. This is particularly obvious in sample #2, with filled pores in *G. ruber* and *N. dutertrei* specimens and connected pores in a *Brizalina sp.* specimen. Samples #2 and #6 have foraminifera displaying isotopic excursions and samples #3 and #6 also contain gypsum crystals.

5. Discussion

5.1. Nature of the Foraminiferal Isotope Variations

[28] The observed similarity between the $\delta^{18}O$ composition of core-top foraminifera and the calculated $\delta^{18}O$ composition of calcite shows that the selected foraminifera species provide a reliable record of the temperature and isotopic composition of surrounding waters (cf., section 3.1, Table 2 and Figure 4). Down-core, the $\delta^{18}O$ profiles for

Figure 3. Number of foraminifera in samples from different batches, as compared to the total organic carbon and gypsum content. (a) Number of planktonic foraminifera picked for isotopic analyses in the first batch of samples processed (Batch #1), which took place between 9 and 19 months after core recovery (*G. ruber*: open blue circles; *N. dutertrei*: filled purple squares). (b) Number of planktonic foraminifera picked in the second batch of samples processed (Batch #2), which took place 10 months after Batch #1. (c) Number of planktonic foraminifera in all samples processed. (d) Number of benthic foraminifera (*Brizalina sp.*: open red crosses; *U. peregrina*: filled orange circles). (e) Total organic carbon content. (f) Gypsum crystals (CaSO₄, 2H₂O) found in the sieved samples. Numbers on the top panel locate the scanning electron microscope samples and the black rectangles in the lower panel show the laminated intervals.
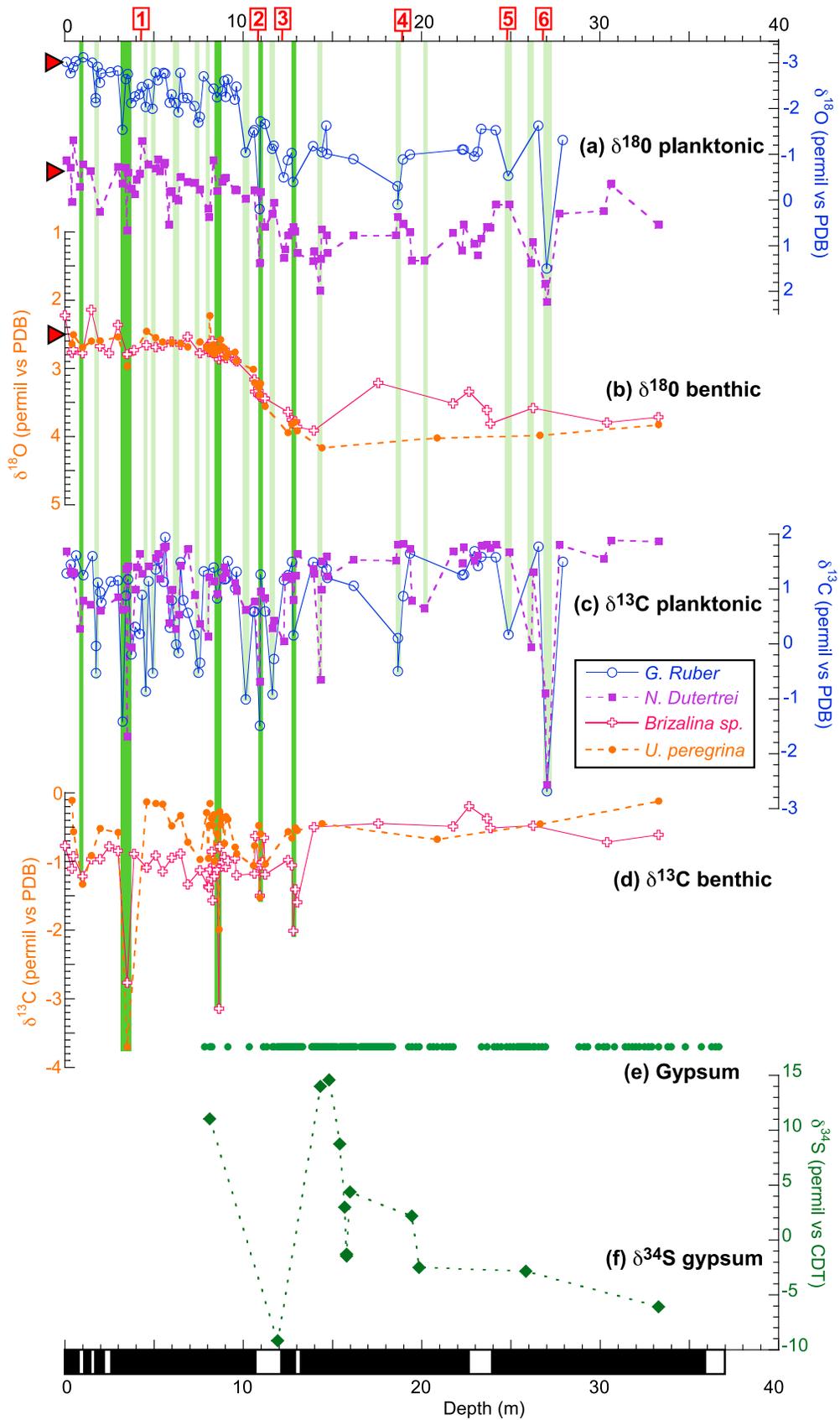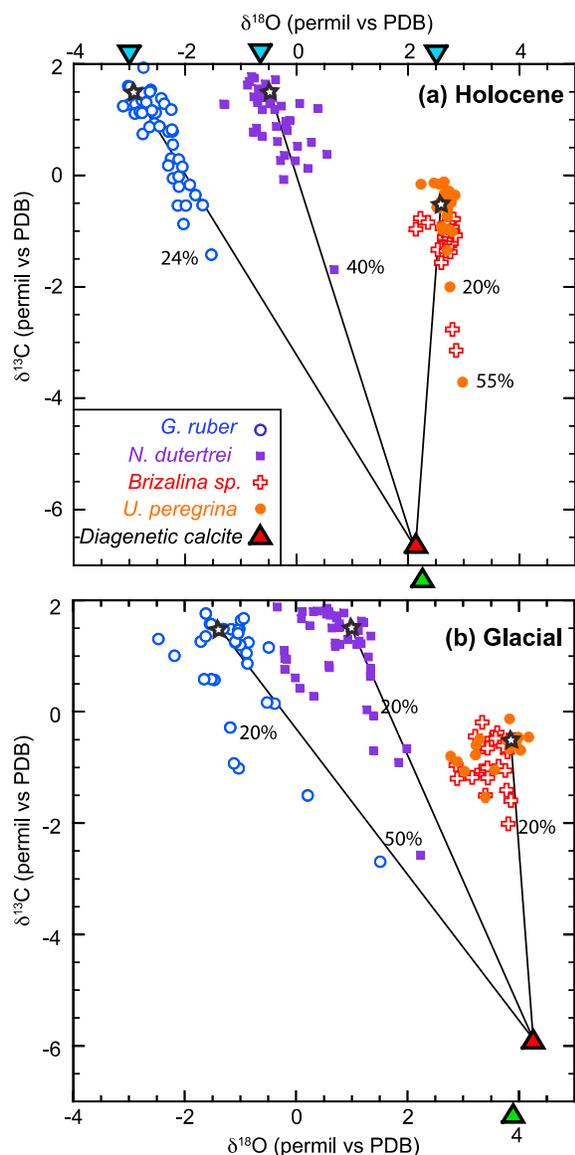
Figure 4

Figure 5. Comparison of $\delta^{18}O$ and $\delta^{13}C$ values for foraminifera to that of inorganic calcite aggregates for (a) the Holocene and (b) the Glacial intervals. $\delta^{18}O$ and $\delta^{13}C$ values for planktonic and benthic foraminifera (legend as in Figure 3), and for calcite aggregates (red triangles). The expected $\delta^{18}O$ for core-top foraminifera is indicated on top of Figure 5a (blue triangles) and that for inorganic calcite formed *in situ* is indicated at the bottom of Figures 5a and 5b (green triangles). Mixing lines between the uncontaminated biogenic calcite (open black stars) and authigenic calcite end-members and percentage of contamination estimated from the mass balance calculations is indicated. See text and Table 2 for further details.

planktonic and benthic foraminifera both exhibit a decrease of ~1.5‰ between 15 and 10 m, which corresponds to the transition between glacial and interglacial conditions, as shown by ^{14}C dating (20–10 ka) (Figure 2). During this transition, the global seawater composition decreased by ~1‰ due to the injection of ^{18}O-depleted waters during the deglacial melting of continental ice sheets [*Labeyrie et al.*, 1987; *Walbroeck et al.*, 2002]. The remaining 0.5‰ decrease can be interpreted as a 2°C warming, in agreement with results from neighboring cores (assuming a negligible change in regional seawater $\delta^{18}O$ composition) [*Kienast et al.*, 2006; *Leduc et al.*, 2007]. Concerning $\delta^{13}C$ (Figure 4), the core-top difference of ~2‰ between planktonic and benthic foraminifera is typical of an oxygen minimum zone [*Berger and Vincent*, 1986]. It reflects the relative enrichment of surface waters in ^{13}C (due to the preferential uptake of ^{12}C during photosynthesis) compared to the bottom and pore waters (where ^{12}C is released during organic matter degradation).

[29] Superimposed on the glacial/interglacial variations, large excursions are observed either in the planktonic records only, or in both the benthic ($\delta^{13}C$) and planktonic ($\delta^{18}O$ and $\delta^{13}C$) records. In all cases, excursions are characterized by strong $\delta^{18}O$ increases (+0.5 to +3‰) and $\delta^{13}C$ decreases (−1.5 to −5‰) that are unlikely to be a consequence of changes in paleoceanographic conditions (Figure 4). Indeed, the co-occurrence of low $\delta^{13}C$, which would indicate a reduction in primary productivity (i.e. present summer conditions) and high $\delta^{18}O$, which would point to more saline/colder waters (i.e. winter-upwelling conditions), is hard to reconcile with the present-day oceanic regime in the Gulf of Tehuantepec.

[30] Benthic $\delta^{13}C$ excursions could reflect strong enrichments of pore waters in ^{12}C where the infaunal foraminifera lived and from which they calcified. Such ^{12}C-rich pore waters could result from enhanced oxidation of organic matter (producing CO_2 of dissolved inorganic carbon ($\delta^{13}C_{DIC}$) of ~−20‰ [*Berger and Vincent*, 1986]) or oxidation of methane (producing lighter $\delta^{13}C_{DIC}$, e.g., up to ~−50‰ in the work of *Torres et al.* [2003]). Both processes strongly affect the pore water composition, and therefore the benthic

Figure 4. Isotopic records. (a) $\delta^{18}O$ records from planktonic foraminifera (legend as in Figure 3). (b) $\delta^{18}O$ records from benthic foraminifera. The red triangles at the left of the profiles indicate the $\delta^{18}O$ composition predicted using modern seawater values and foraminifera-based paleotemperature equations (see Table 2 and text for details). (c) $\delta^{13}C$ records from planktonic foraminifera; (d) $\delta^{13}C$ records from benthic foraminifera; (e) Gypsum crystals and (f) $\delta^{34}S$ record from gypsum crystals.
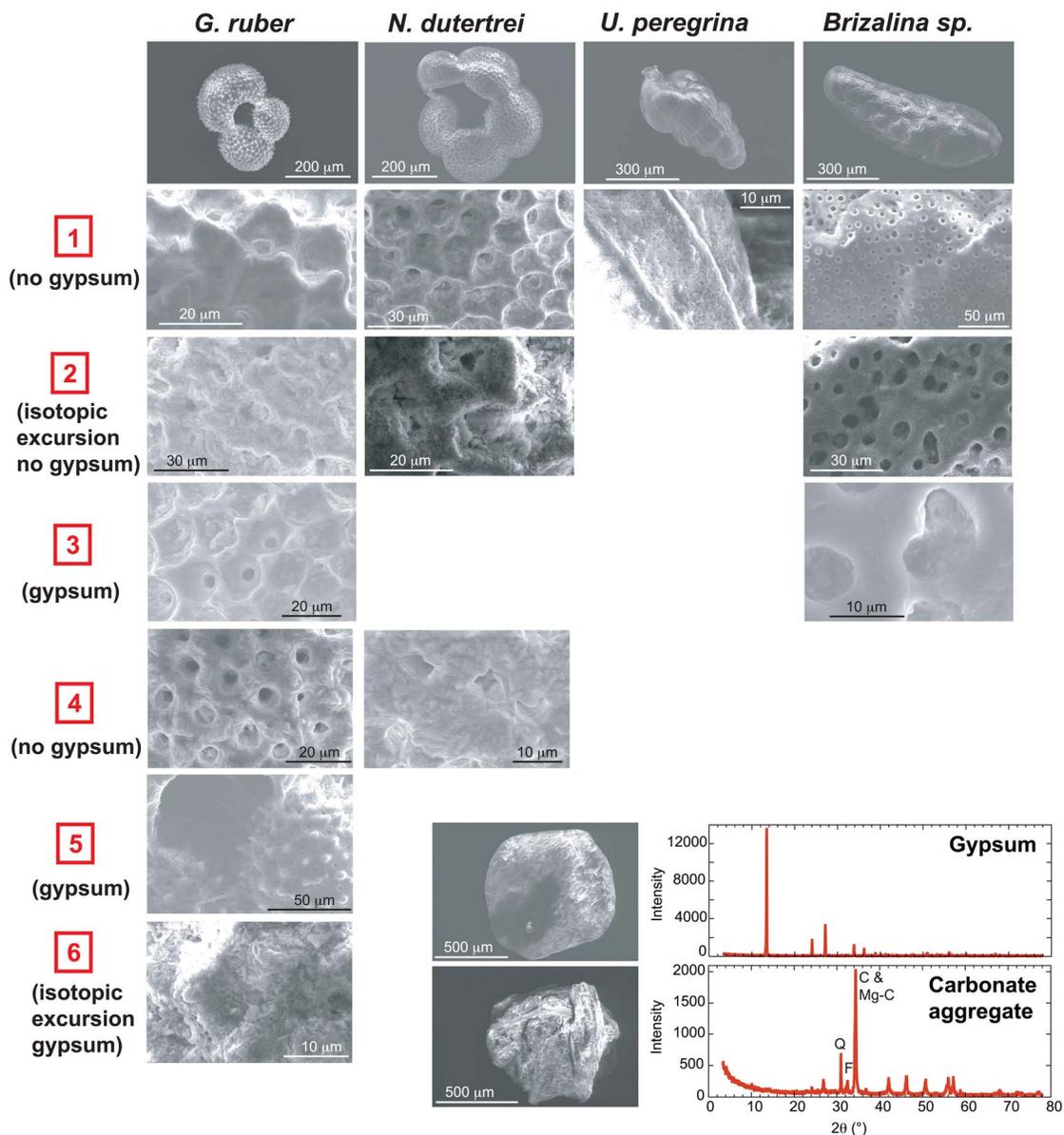
Figure 6. Main panel: Scanning electron microscope (SEM) pictures of specimens and details of tests of *G. ruber*, *N. dutertrei*, *U. peregrina*, *Brizalina sp.*. Samples taken at 4.18 m (#1), 10.92 m (#2), 12.91 m (#3), 18.96 m (#4), 24.84 m (#5) and 26.54 m (#6). Re-crystallization processes indicated by filled pores in #2, #3 and #6 and dissolution processes identified by connected pores in #2, #3 and #4. Excellent preservation state in #5 indicated by the thin calcite spines of *G. ruber*. Small panel: SEM pictures and X-ray diffraction spectra of a gypsum crystal (from sample #3) and an inorganic calcite aggregate (from sample #5). Minerals identified: quartz (Q), feldspar (F), calcite (C) and magnesian-calcite (Mg-C).

foraminifera isotopic composition. It was suggested that destabilization of gas hydrates (which are stable in the present pressure and temperature fields at the core site), and subsequent release and oxidation of large amounts of methane could also affect the seawater composition, and therefore the isotope composition of both benthic and planktonic foraminifera [e.g., *de Garidel-Thoron et al.*, 2004].

However, in core MD02-2520, some isotopic excursions are observed only in planktonic foraminifera (i.e., not in benthic foraminifera) (lighter green underlines in Figure 4), which cannot be explained by sea- or pore water ^{12}C-enrichments due to enhanced organic matter oxidation or methane oxidation. We infer instead that the isotopic excursions observed in the foraminiferal record

presented here are most likely related to diagenetic or post-sampling processes.

5.2. Processes Altering the Primary Isotopic Signals

5.2.1. Dissolution of Ontogenetic Calcite

[31] As shown in previous studies, the layers of ontogenetic calcite are preferentially dissolved when planktonic foraminifera are placed in a corrosive environment [*Berger and Killingley*, 1977]. The tests then carry the signature of the gametogenic calcite that is formed in deeper waters (^{18}O-enriched and ^{13}C-depleted) compared to the water masses in which the ontogenetic calcite forms, which leads to higher $\delta^{18}O$ and lower $\delta^{13}C$ values [*Duplessy et al.*, 1981]. Thus, this process could explain the isotopic excursions identified in planktonic records, as well as the traces of dissolution observed for several foraminifera (e.g., *Brizalina sp.* specimen in samples #2 and in #3, Figure 6), and the lack of foraminifera between 37 and 15 m.

[32] However, this process cannot account for the isotopic excursions observed in the *G. ruber* and in the benthic records. First, *Caron et al.* [1990] showed that *G. ruber* does not add significant gametogenic calcite and dissolution processes, if occurring, would not affect the isotopic ratios. Second, this process cannot account for the benthic isotopic excursions, since the ontogenetic and the gametogenic calcite layers of benthic foraminifera do not carry significantly different isotopic signatures. Indeed, migrations of benthic foraminifera in the sediments are mostly controlled by environmental conditions, rather than by the life cycle [*McCorkle et al.*, 1997]. Therefore, even if calcite dissolution occurred, it is unlikely to be responsible for the observed isotopic excursions. Additionally, since the benthic tests are generally more resistant toward dissolution [*Kucera et al.*, 1997], this is an unlikely explanation for the lack of benthic foraminifera at horizons where planktonic foraminifera are present (e.g., in glacial sediments, Figure 3). We therefore conclude that although calcite dissolution was observed on certain foraminifera (Figure 6), it remains a minor process in core MD02-2520 and its effects on the isotopic record are negligible.

5.2.2. Precipitation of Authigenic Calcite

[33] The SEM images reveal the presence of inorganic (authigenic) calcite in pores of the foraminifera (e.g., *N. dutertrei* specimen in sample #2, Figure 6) and as mm-scale aggregates (sample #5, Figure 6).

The precipitation of authigenic calcite can drastically modify isotopic signals [*Reuning et al.*, 2005]. This process generally affects the planktonic more than the benthic foraminifera, since: i) the isotopic composition and temperature of surface seawater differs greatly from that of pore water and, ii) planktonic foraminifera are more porous than benthic foraminifera, and therefore provide a larger area for precipitation [*Pearson et al.*, 2001]. In particular, the $\delta^{18}O$ of authigenic calcite is very different from the $\delta^{18}O$ of uncontaminated planktonic foraminifera, due to large differences in temperature between the surface waters and the pore waters.

[34] As can be seen from Figure 5, the isotope composition of a number of planktonic and benthic foraminifera deviates toward the isotopic composition of inorganic calcite and hints toward precipitation of inorganic calcite on the tests. The $\delta^{13}C$ of both planktonic and benthic foraminifera is affected by this process and the $\delta^{18}O$ of planktonic foraminifer is more affected than that of benthic foraminifera. The measured $\delta^{18}O$ for calcite aggregates is in accordance with the predicted composition of inorganic calcite formed in similar conditions in the sediments, following the equation established by *Kim and O'Neil* [1997] (Table 2 and Figure 5). Using the isotope composition of calcite aggregates and uncontaminated foraminifera, it is possible to estimate the amount of authigenic calcite added on the tests. We use the equation

$$Am = \frac{\delta_{Meas} - \delta_{Biog}}{\delta_{Authi} - \delta_{Biog}} * 100,$$

where Am is the mass balanced amount of authigenic calcite added to the test (in %), δ_{Meas} is the measured isotopic composition of the foraminifera, δ_{Biog} is the isotopic composition of the uncontaminated foraminifera and δ_{Authi} is the isotopic composition of the authigenic calcite (all in ‰). The end-members for uncontaminated foraminifera were determined by: i) using the core-top $\delta^{18}O$ for the Holocene and the core-top $\delta^{13}C$ values for both intervals, and ii) adding 1.5‰ to the core-top $\delta^{18}O$ values for the Glacial (see section 5.1). Linear mixing is expected between the biogenic calcite and authigenic calcite end-members, as the ratio of carbon to oxygen is theoretically identical in both end-members (i.e., C/O ∼1/3) (Figure 5) [*Faure*, 1986].

[35] Mass balance estimates indicate that a 10–50 % contamination by inorganic calcite precipitation would explain the $\delta^{13}C$ and $\delta^{18}O$ excursions. Our calculations therefore indicate that the isotopic

Table 3. Biochemicals Reactions as Cited in the Text

Reaction	Number
Organic Matter Mineralization	
$CH_2O + O_2 \rightarrow CO_2 + H_2O$	(1)
$5CH_2O + 4NO_3^- \rightarrow HCO_3^- + 2N_2 + CO_2 + 3H_2O$	(2)
$CH_2O + 7CO_2 + 4Fe(OH)_3 \rightarrow 4Fe^{2+} + 8HCO_3^- + 3H_2O$	(3)
$2CH_2O + SO_4^{2-} \rightarrow H_2S + 2HCO_3^-$	(4)
Anaerobic Oxidation of Methane	
$CH_4 + SO_4^{2-} \rightarrow HS^- + HCO_3^- + H_2O$	(5)
Sulfide Precipitation	
$Fe^{2+} + H_2S \rightarrow FeS + 2H^+$	(6)
$FeS + H_2S \rightarrow FeS_2 + H_2$	(7)
Chemical Sulfide Oxidation	
$4FeS_2 + 9O_2 + 6H_2O \rightarrow 4FeOOH + 4SO_4^{2-} + 8H^+$	(8)
$H_2S + 2FeOOH + 5H^+ \rightarrow 2Fe^{2+} + 4H_2O + S^0$	(9)
$4H_2S + 4MnO_2 \rightarrow 4S^0 + 4Mn^{2+} + 8OH^-$	(10)
$FeS + 1.5MnO_2 + 3H^+ \rightarrow S^0 + Fe(OH)_3 + 1.5Mn^{2+}$	(11)
Elemental Sulfur Disproportionation	
$4S^0 + 4H_2O \rightarrow SO_4^{2-} + 3H_2S + 2H^+$	(12)
Sulfide Oxidation and Disproportionation	
$H_2S + 4MnO_2 + 2H_2O \rightarrow 4Mn^{2+} + SO_4^{2-} + 6OH^-$	(13)
$FeS_2 + 7.5MnO_2 + 11H^+ \rightarrow Fe(OH)_3 + 2SO_4^{2-} + 7.5Mn^{2+} + 4H_2O$	(14)

excursions likely result from precipitation of authigenic calcite. However, the amounts calculated to produce the larger excursions (e.g., the ones at ∼6, ∼8 and ∼27 m) were not observed on the foraminifer tests (Figure 6). This might be related to local changes in the isotopic signature of the inorganic calcite, which have been shown to reach $\delta^{13}C$ values of −15‰ in organic-rich sediments [*Irwin et al.*, 1977].

5.3. Diagenetic or Post-Sampling Processes?

[36] Although apparently contradictory, the co-occurrence of dissolution and precipitation processes was identified in some samples (e.g., #2, Figure 6). Additionally, gypsum crystals were identified in several samples, as well as inorganic calcite (Figure 2). Such processes may happen either during storage of sediments after core recovery, or during early diagenesis. All biogeochemical reactions mentioned in the following sections are numbered and listed in Table 3.

5.3.1. Transformations Occurring During Sediment Storage

[37] Laminated sediments from the eastern Pacific OMZ are known to contain large amounts of reduced sulfur species such as hydrogen sulfide and solid-phase iron sulfides (e.g., mackinawite FeS, pyrite FeS$_2$) [*Reimers et al.*, 1996]. When placed in an oxic environment (i.e., if oxygen diffuses into the sediments after core recovery), these reduced sulfur species may be oxidized stepwise to produce SO_4^{2-}, elemental S and H^+ (equation (8) in Table 3). The organic matter that was preserved in the sediments can also be oxidized to produce CO_2 (equation (1)), which is incorporated in the dissolved carbonate pool. These oxidation processes can lead to a local decrease in pore water pH that favors the dissolution of biogenic carbonates, as already observed by *Schnitker et al.* [1980] and *Self-Trail and Seefelt* [2005] for sediments freshly recovered and dried in the presence of oxygen. Both studies also reported the formation of gypsum, resulting from the presence of dissolved calcium and sulfate in the pore space. In core MD02-2520, the $\delta^{34}S$ values of gypsum range from −10 to +15‰, which is lighter than seawater sulfate (∼20‰ [*Rees et al.*, 1978]). Isotopically light sulfate could originate from the oxidation of reduced sulfide species, which are enriched in ^{32}S due to the preferential uptake of the light isotope during sulfate reduction [*Jørgensen*, 1990]. Unfortunately, the isotopic composition of dissolved sulfate and sulfide, and solid phase sulfide is not available for core MD02-2520. However, studies of similar
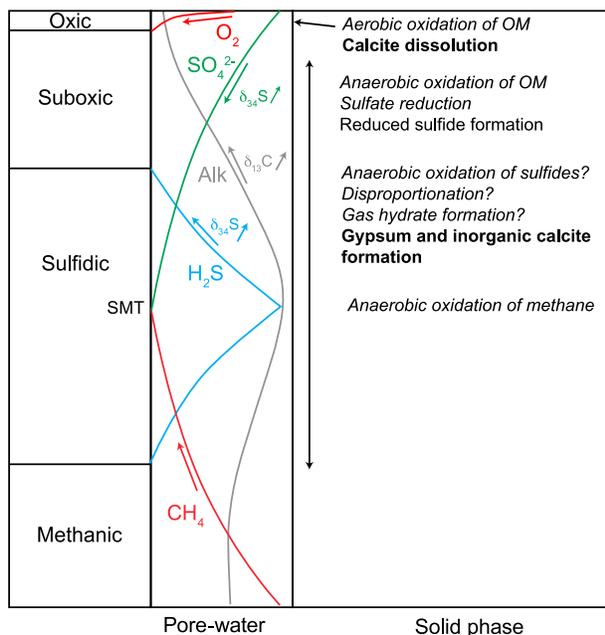
Figure 7. Schematic sediment column for core site MD02-2520, with (right column) geochemical zonation, (center) pore water chemical profiles (central column), with diffusion directions (arrows) and changes in isotopic composition, and (left column) transformations occurring within the solid phase.

sedimentological settings (like the laminated sediments of the Santa Barbara Basin, which have similar accumulation rates and TOC contents) demonstrate that dissolved and solid phase sulfide species tend to have negative $\delta^{34}S$ values ($\sim-20\permil$ for H_2S and FeS_2 [*Brüchert and Pratt*, 1996]). Therefore, the gypsum crystals that were analyzed for the present study may potentially reflect post-sampling sulfide oxidation, with additional contributions from isotopically heavier (residual) seawater sulfate and isotopically lighter organic sulfur (with $\delta^{34}S$ values ranging from -5 to $-30\permil$ [*Werne et al.*, 2008]).

[38] However, post-sampling oxidation of sulfide and organic matter generally results in the dissolution of biogenic carbonate [*Schnitker et al.*, 1980; *Self-Trail and Seefelt*, 2005], which is a minor process in core MD02-2520 (section 5.2.1). This suggests that the calcite aggregates most probably formed during early diagenesis. *Self-Trail and Seefelt* [2005] demonstrated that the amount of carbonaceous fossils dissolved increases with drying time. In other words, the longer sediments are put in contact with oxygen, the more biogenic carbonate will be dissolved. This is not observed in our case: the foraminiferal assemblage and

quantity did not vary between the two batches processed, nor did the amount of gypsum despite a few months elapsing between the batches (Figure 2 and section 3.1). Therefore, although we cannot rule out post-sampling oxidation, this effect seems to be of minor importance in core MD02-2520.

5.3.2. Transformations Occurring During Early Diagenesis

[39] In marine sediments, two main processes largely control the carbonate system of pore waters, and therefore influence the dissolution of biogenic carbonates and precipitation of inorganic calcite: i) the mineralization of organic matter and ii) the anaerobic oxidation of methane (AOM) [*Jørgensen and Kasten*, 2006]. The dissolution of biogenic carbonates is generally induced by the mineralization of organic matter in the presence of oxygen (equation (1)), which leads to a release of CO_2 into the pore waters [*Jahnke et al.*, 1997; *Pfeifer et al.*, 2002; *Volbers and Henrich*, 2002]. In laminated sediments from the eastern Pacific OMZ, the oxic zone is restricted to the upper few cm (sometimes even to the upper few mm) of sediments deposited [*Reimers et al.*, 1996] (Figure 7). Additionally, the precipitation of iron monosulfides produces protons that might lower the pore water pH (equation (6)) and lead to dissolution of biogenic carbonates. However, in sediments containing a large amount of iron oxides (which is the case for core MD02-2520 [cf. *Blanchet*, 2006]), iron liberation reactions dominate in the suboxic zone and determine the pore water pH (equation (3)), which can reach particularly high values (like in the Santa Barbara Basin, where pH are higher than 8) [*Reimers et al.*, 1996]. Therefore, we consider that carbonate dissolution was restricted to the oxic zone and is a minor diagenetic process at the site of core MD02-2520.

[40] Precipitation of inorganic calcite is tightly linked to pore water alkalinity, which generally increases in organic-rich marine sediments as a result of anaerobic organic matter mineralization and AOM (equations (2)–(5)). When oxygen is completely depleted in the pore waters, other oxidants such as nitrate (equation (2)), iron and manganese oxides (equation (3)) or sulfate (equation (4)) are used to mineralize the organic matter, which releases carbonate ions into the pore water and increases alkalinity [*Reimers et al.*, 1996]. Such reactions might induce authigenic calcite precipitation in the suboxic and sulfidic zones (Figure 7).

In the suboxic zone, the pore water $\delta^{13}C_{DIC}$ is largely determined by the $\delta^{13}C$ signature of the organic matter (~-20‰) [*Stott et al.*, 2002]. Around the SMT, the process of AOM results in an increase in pore water alkalinity and a decrease in $\delta^{13}C_{DIC}$, due to contribution of methane-derived carbonate ions with $\delta^{13}C_{DIC}$ sometimes reaching -50‰ [*Torres et al.*, 1996]. Precipitation of inorganic calcite around the SMT has been well-documented [e.g., *Bohrmann et al.*, 1998; *Greinert et al.*, 2002; *Nöthen and Kasten*, 2011], but such calcite generally has lighter $\delta^{13}C$ signatures than the aggregates from core MD02-2520 (e.g., ~-15‰ in organic-rich sediments from the Chilean upwelling region [*Treude et al.*, 2005]). Authigenic calcite formed in methane seeps is also known to overprint the fossil foraminiferal record (due to precipitation of authigenic calcite on the tests) but it also carries $\delta^{13}C$ values much lower than those obtained for core MD02-2520 (-22 to -51‰ [*Torres et al.*, 2003; *Cook et al.*, 2011]). Unfortunately, pore water $\delta^{13}C_{DIC}$ profiles are not available for our study site, thus it is impossible to precisely determine the formation depth of the observed inorganic calcite. We hypothesize that it formed in the suboxic zone and at the top of the sulfidic zone, mostly as a result of anaerobic oxidation of organic matter with a minor contribution from carbonates produced during AOM (Figure 7).

[41] The formation of gypsum crystals in marine sediments has been reported and described in only a few studies [*Siesser and Rogers*, 1976; *Briskin and Schreiber*, 1978; *Muza and Sherwood*, 1983; *Hoareau et al.*, 2011]. In order to characterize the sedimentary context where gypsum might precipitate, *Hoareau et al.* [2011] calculated the gypsum saturation index for numerous ODP/IODP cores using the available pore water data. They reported that gypsum saturation was observed in the presence of evaporitic horizons or volcanogenic material (able to provide sufficient calcium and sulfate ions to the pore water). The sediments of core MD02-2520 are barren of evaporitic or volcanogenic material, and pore water data are unfortunately not available. It is therefore impossible to precisely pin-point the mechanism leading to gypsum formation. However, in the following we will review the potential processes that could lead to local supersaturation of pore waters with respect to gypsum. Such processes can involve either: i) oxidation of the reduced sulfide species that could provide sufficient sulfate ions to form gypsum, or ii) an increase of pore water salinity that would be sufficient to reach gypsum supersaturation.

[42] Sulfide oxidation in anoxic marine sediments is an important component of the biogeochemical sulfur cycle, and can significantly contribute to the dissolved pore water sulfate pool [*Jørgensen and Kasten*, 2006; *Riedinger et al.*, 2010]. *Fossing and Jorgensen* [1990] have for instance observed a complete re-oxidation of radio-labeled mono-sulfides (FeS) and elemental sulfur (S^0) to sulfate in anoxic sediments. The complete re-oxidation of sulfur species (of various oxidation states) to sulfate generally involves a suite of chemical and micro-bially mediated chain reactions. The H_2S produced during either organoclastic sulfate reduction or AOM might either: i) react with solid-phase Fe(III) oxides, dissolved (Fe^{2+}) iron or iron monosulfides to form iron sulfide minerals of various oxidation states (FeS or FeS_2, equations (6) and (7)), or ii) be re-oxidized by oxidants such as iron and manganese oxides, which gives rise to sulfide species of intermediate oxidation state such as elemental sulfur (S^0) (equations (9)–(11)) [*Thamdrup et al.*, 1994]. *Schippers and Jørgensen* [2001] have shown that manganese dioxide is a powerful chemical oxidant, that is able to oxidize mono-sulfides to elemental sulfur (equations (10) and (11)). Oxidation of sulfur species coupled to the reduction of iron (oxyhydro)oxides has also been demonstrated to occur in sediments of the Nankai Trough [*Riedinger et al.*, 2010]. When accompanied by microbial processes such as elemental sulfur disproportionation, monosulfides as well as pyrite can be reoxidized to sulfate (equations (13) and (14)) [*Aller and Rude*, 1988; *Schippers and Jørgensen*, 2001]. Sulfur disproportionation is a type of inorganic fermentation that occurs in anoxic sediments rich in intermediate sulfur species such as elemental sulfur or thiosulfate ($S_2O_3^{2-}$). In this way, a quarter of the elemental sulfur is oxidized to sulfate while the remaining three quarters return to the sulfide pool (equation (12)) [*Jørgensen and Kasten*, 2006]. In core MD02-2520, the glacial sediments are enriched in iron (oxyhydr)oxides [*Blanchet*, 2006], which were recently shown to favor oxidative sulfur processes [*Riedinger et al.*, 2010; *Holmkvist et al.*, 2011a, 2011b]. Such processes could therefore lead to the accumulation of sulfate in micro-environments in the pore water and could explain the co-existence of pyrite and gypsum in the glacial sediments of core MD02-2520.

[43] Finally, we speculate that local increases in pore water salinity, sufficient enough to reach gypsum saturation state, might also occur as a result of gas hydrate formation. During gas hydrate formation, ions are excluded from the hydrate

structure and lead to the formation of residual brines either in the sediments surrounding the gas hydrates or in the pore space of the hydrates [*Ussler and Paull*, 1995]. Site MD02-2520 lies within the gas hydrate stability field and the presence of *in situ* gas hydrates was evidenced by sediment expansions during core recovery (i.e., section 3.1). It is therefore possible that oversaturation and thus precipitation of gypsum (and possibly also authigenic calcite) has been induced *in situ* during formation of gas hydrates below the SMT where iron sulfides are known to precipitate [e.g., *Kasten et al.*, 1998; *Jørgensen et al.*, 2004].

6. Summary and Conclusions

[44] Our data for core MD02-2520 show that the carbon and oxygen isotope records for planktonic and benthic foraminifera provide a reliable archive of present and past oceanographic conditions (mostly at glacial/interglacial scale). However, the record is characterized by large excursions (reaching +3‰ in $\delta^{18}O$ and $-5‰$ in $\delta^{13}C$) that point, together with the presence of inorganic calcite aggregates and gypsum crystals, to substantial diagenetic overprint. Scanning electron microscopy reveals the co-occurrence of dissolution of the primary (biogenic) calcite and precipitation of secondary (authigenic) calcite on the tests. We propose that precipitation processes are dominant over dissolution processes at site MD02-2520, as shown by the presence of dissolution-sensitive foraminifera in layers barren of dissolution-resistant foraminifera and by mass balance calculations for authigenic calcite coatings on the tests. The dominance of precipitation over dissolution, as well as the absence of time-related modification of the foraminiferal assemblage and gypsum contents during storage, are best explained by diagenetic processes rather than by transformations occurring after retrieval and during sediment storage.

[45] Due to the lack of pore water geochemical data for core MD02-2520, the precise diagenetic processes responsible for calcite and gypsum precipitation are not readily resolvable. However, the carbon isotope composition for inorganic calcite aggregates ($\delta^{13}C \sim -6‰$) indicates that the carbonate ions originate for the most part from anaerobic oxidation of organic matter, potentially coupled with the anaerobic oxidation of methane. The sulfur isotope composition of gypsum crystals ($\delta^{34}S$ from -10 to $+15‰$) is lighter than the $\delta^{34}S$ of seawater sulfate, suggesting a significant contribution from sulfate originating from the oxidation of

organic matter and authigenic sulfide compounds. We speculate that both organic matter and sulfides were oxidized by metal (manganese and iron) oxides to form carbonate ions and intermediate sulfur species. These sulfur species might have been subsequently oxidized through microbially mediated sulfur disproportionation to produce enough sulfate to reach gypsum supersaturation. A further contribution may result from local increase in pore water salinity due to formation of gas hydrates, which could potentially lead to super-saturation of pore waters with respect to gypsum and induce the formation of gypsum with heavier $\delta^{34}S$ signatures.

[46] Our study demonstrates the impact of inorganic calcite precipitation on the isotopic composition of foraminifera. This effect has already been identified [e.g., *Killingley*, 1983] but was generally related to formation of inorganic calcite in relation to anaerobic methane oxidation at methane/cold seeps [*Torres et al.*, 2003; *Cook et al.*, 2011] and in methane-rich sediments of high-productivity areas [*Treude et al.*, 2005]. Here, we show that inorganic calcite formation resulting from anaerobic oxidation of organic matter can also alter the proxy record. These processes are favored by high sedimentary organic contents and low pore water oxygen contents. The elemental and isotopic composition of foraminifera in such sediments should therefore be interpreted with care. Although more work is needed to assess the relationships between calcite and gypsum formation, the presence of gypsum crystals in the sediments (which is generally neglected or attributed to post-sampling oxidation) may imply significant diagenetic overprinting of the primary oceanic record.

Acknowledgments

References

Aller, R., and P. Rude (1988), Complete oxidation of solid phase sulfides by manganese and bacteria in anoxic marine sediments, *Geochim. Cosmochim. Acta*, *52*, 751–765.

Bard, E., F. Rostek, and G. Ménot-Combes (2004), Radiocarbon calibration beyond 20,000 ^{14}C yr by means of planktonic foraminifera of the Iberian Margin, *Quat. Res.*, *61*, 204–214.

Basak, C., E. E. Martin, K. Horikawa, and T. M. Marchitto (2010), Southern Ocean source of ^{14}C-depleted carbon on the North Pacific Ocean during the last deglaciation, *Nat. Geosci.*, *3*, 770–773.

Beaufort, L., T. Pedersen, M. Machain-Castillo, and the Cruise Participants (2002), Marges Ouest Nord Américaines (MONA) cruise report, MD126-IMAGESVIII, *Cruise Rep. MD 126*, Inst. Paul Emile Victor, Plouzané, France.

Bemis, B. E., H. J. Spero, J. Bijma, and D. W. Lea (1998), Reevaluation of the oxygen isotopic composition of planctonic foraminifera: Experimental results and revised paleotemperature equations, *Paleoceanography*, *13*, 150–160.

Benson, L., J. C. Liddicoat, J. Smoot, A. Sarna-Wojcicki, R. Negrini, and S. Lund (2003), Age of the Mono Lake excursion and associated tephra, *Quat. Sci. Rev.*, *22*, 135–140.

Benway, H. M., and A. C. Mix (2004), Oxygen isotopes, upper-ocean salinity, and precipitation sources in the eastern tropical Pacific, *Earth Planet. Sci. Lett.*, *224*, 493–507.

Berger, R., R. E. Taylor, and W. F. Libby (1966), Radiocarbon content of marine shells from the California and Mexican west coast, *Science*, *153*, 864–866.

Berger, W. H., and J. S. Killingley (1977), Glacial-Holocene transition in deep-sea sediments: Selective dissolution and the stable isotope signal, *Science*, *197*, 563–566.

Berger, W. H., and E. Vincent (1986), Deep-sea carbonates: Reading the carbon-isotope signal, *Geol. Rundsch.*, *75*, 249–269.

Blanchet, C. L. (2006), Variabilités climatiques et océaniques du dernier cycle Glaciaire-Interglaciaire. propriétés magnétiques et géochimiques des sédiments de la marge nord-ouest Américaine subtropicale, PhD thesis, Univ. Paul Cézanne Aix-Marseille III, Aix-Marseille, France.

Bohrmann, G., J. Greinert, E. Suess, and M. Torres (1998), Authigenic carbonates from the Cascadia subduction zone and their relation to gas hydrate stability, *Geology*, *26*, 647–650.

Briskin, M., and C. Schreiber (1978), Authigenic Gypsum in marine sediments, *Mar. Geol.*, *28*, 37–49.

Brüchert, V., and L. M. Pratt (1996), Contemporaneous early diagenetic formation of organic and inorganic sulfur in estuarine sediments from St Andrew Bay, Florida, USA, *Geochim. Cosmochim. Acta*, *60*, 2325–2332.

Caron, D. A., O. R. Anderson, J. L. Lindsey, W. W. Faber Jr., and E. L. Lim (1990), Effects of gametogenesis on test structure and dissolution of some spinose planktonic foraminifera and implications for test preservation, *Mar. Micropaleontology*, *16*, 93–116, doi:10.1016/0377-8398(90)90031-G.

Cartapanis, O., K. Tachikawa, and E. Bard (2011), Northeastern pacific oxygen minimum zone variability over the past 70 kyr: Impact of biological production and oceanic ventilation, *Paleoceanography*, *26*, PA4208, doi:10.1029/2011PA002126.

Conkright, M. E., R. A. Locarnini, H. E. Garcia, T. D. O'Brien, T. P. Boyer, C. Stephens, and J. I. Antonov (2002), World Ocean Atlas 2001: Objective analyses, data statistics, and figures, CD-ROM documentation, technical report, Natl. Oceanogr. Data Cent., Silver Spring, Md.

Cook, M., L. D. Keigwin, D. Birgel, and K.-U. Hinrichs (2011), Repeated pulses of vertical methane flux recorded in glacial sediments from the southeast Bering Sea, *Paleoceanography*, *26*, PA2210, doi:10.1029/2010PA001993.

de Garidel-Thoron, T., L. Beaufort, F. Bassinot, and P. Henry (2004), Evidence for large methane releases to the atmosphere from deep-sea gas-hydrate dissociation during the last glacial period, *Proc. Natl. Acad. Sci. U. S. A.*, *101*, 9187–9192.

Dickens, G. R. (2001), Sulfate profiles and barium fronts in sediments on the Blake Ridge: Present and past methane fluxes through a large gas hydrate reservoir, *Geochim. Cosmochim. Acta*, *65*, 529–543.

Dunkley-Jones, T., and P. R. Brown (2007), Post-sampling dissolution and the consistency of nannofossils diversity measures: A case study from freshly cored sediments of coastal Tanzania, *Mar. Micropaleontology*, *62*, 254–268.

Duplessy, J.-C., P.-L. Blanc, and A. W. H. Bé (1981), Oxygen-18 enrichment of planktonic foraminifera due to gametogenic calcification below the euphotic zone, *Science*, *213*, 1247–1250.

Duplessy, J.-C., L. Labeyrie, A. Juillet-Leclerc, F. Maitre, J. Duprat, and M. Sarnthein (1991), Surface salinity reconstructions of the North Atlantic Ocean during the last glacial maximum, *Oceanol. Acta*, *14*, 311–324.

Emiliani, C. (1955), Pleistocene temperatures, *J. Geol.*, *63*, 538–578.

Färber-Lorda, J., M. F. Lavin, and M. A. Guerrero-Ruiz (2004), Effect of wind forcing on the trophic conditions, zooplankton biomass and krill biochemical composition in the Gulf of Tehuantepec, *Deep Sea Res., Part II*, *51*, 601–614.

Faure, G. (1986), *Principles of Isotope Geochemistry*, John Wiley, New York.

Fossing, H., and B. Jorgensen (1990), Oxidation and reduction of radiolabeled inorganic sulfur compounds in an estuarine sediment, Kysing Fjord, Denmark, *Geochim. Cosmochim. Acta*, *54*, 2731–2742.

Greinert, J., S. M. Bollwerk, A. Derkachev, G. Bohrmann, and E. Suess (2002), Massive barite deposits and carbonate mineralization in the Derugin Basin, Sea of Okhotsk: precipitation processes at cold seeps, *Earth Planet. Sci. Lett.*, *203*, 165–180.

Guillou, H., B. Singer, C. Laj, C. Kissel, S. Scaillet, and B. R. Jicha (2004), On the age of the Laschamp geomagnetic excursion, *Earth Planet. Sci. Lett.*, *227*, 331–343.

Hendy, I. L., and T. F. Pedersen (2006), Oxygen minimum zone expansion in the eastern tropical North Pacific during deglaciation, *Geophys. Res. Lett.*, *33*, L20602, doi:10.1029/2006GL025975.

Hoareau, G., C. Monnin, and F. Odonne (2011), The stability of gypsum in marine sediments using the entire ODP/IODP porewater composition database, *Mar. Geol.*, *279*(1–4), 87–97.

Holmkvist, L., T. G. Ferdelman, and B. B. Jørgensen (2011a), A cryptic sulfur cycle driven by iron in the methane zone of marine sediments (Aarhus Bay, Denmark), *Geochim. Cosmochim. Acta*, *75*, 3581–3599.

Holmkvist, L., A. Kamyshny Jr., C. Vogt, K. Vamvakopoulos, T. G. Ferdelman, and B. B. Jørgensen (2011b), Sulfate reduction below the sulfate-methane transition in Black Sea sediments, *Deep Sea Res., Part I*, *58*, 493–504.

Hughen, C. A., S. Lehman, J. Southon, J. Overpeck, O. Marchal, C. Herring, and J. Turnbull (2004), ^{14}C activity and global carbon cycle changes over the past 50,000 years, *Science*, *303*, 202–207.

Irwin, H., C. Curtis, and M. Coleman (1977), Isotopic evidence for source of diagenetic carbonates formed during burial of organic-rich sediments, *Nature*, *269*, 209–213.

Jahnke, R. A., D. B. Craven, D. C. McCorkle, and C. E. Reimers (1997), CaCO₃ dissolution in California continental margin sediments: The influence of organic matter remineralization, *Geochim. Cosmochim. Acta*, *61*, 3587–3604.

Jørgensen, B. B. (1990), A thiosulfate shunt in the sulfur cycle of marine sediments, *Science*, *249*, 152–154.

Jørgensen, B. B., and S. Kasten (2006), Sulfur cycling and methane oxidation, in *Mar. Geochem.*, edited by H. D. Schulz and M. Zabel, pp. 271–310, Springer, Berlin.

Jørgensen, B. B., M. E. Böttcher, H. Lueschen, L. N. Neretin, and I. I. Volkov (2004), Anaerobic methane oxidation and a deep H₂S sink generate isotopically heavy sulfides in Black Sea sediments, *Geochim. Cosmochim. Acta*, *68*, 2095–2118.

Kalnay, E., et al. (1996), The NCEP/NCAR 40-year reanalysis project, *Bull. Am. Meteorol. Soc.*, *77*, 437–471.

Kasten, S., T. Freudenthal, F. X. Gingele, T. von Dobeneck, and H. D. Schulz (1998), Simultaneous formation of iron-rich layers at different redox boundaries in sediments of the Amazon Deep-Sea Fan, *Geochim. Cosmochim. Acta*, *62*, 2253–2264.

Kienast, M., S. S. Kienast, S. E. Calvert, T. I. Eglington, G. Mollenhauer, R. François, and A. C. Mix (2006), Eastern Pacific cooling and Atlantic overturning circulation during the last deglactiation, *Nature*, *443*, 346–349.

Killingley, J. S. (1983), Effects of diagenetic recrystallization on ¹⁶O/¹⁸O values of deep-sea sediments, *Nature*, *301*, 594–597.

Kim, S. T., and J. R. O'Neil (1997), Equilibrium and non-equilibrium oxygen isotope effects in synthetic carbonates, *Geochim. Cosmochim. Acta*, *61*, 3461–3475.

Kucera, M., B. A. Malmgren, and U. Sturesson (1997), Foraminiferal dissolution at shallow depths of the Walvis Ridge and Rio Grande Rise during the latest Cretaceous: Inferences for deep-water circulation in the South Atlantic, *Palaeogeogr. Palaeoclimatol. Palaeoecol.*, *129*, 195–212.

Labeyrie, J., J.-C. Duplessy, and P.-L. Blanc (1987), Variations of mode of formation and temperature of oceanic deep waters over the past 125 000 years, *Nature*, *327*, 477–482.

Lacan, F., and C. Jeandel (2001), Tracing Papua New Guinea imprint on the central Equatorial Pacific Ocean using neodymium isotopic compositions and Rare Earth Element patterns, *Earth Planet. Sci. Lett.*, *186*, 497–512.

Leduc, G., L. Vidal, K. Tachikawa, F. Rostek, C. Sonzogni, L. Beaufort, and E. Bard (2007), Moisture transport across Central America as positive feedback on abrupt climatic changes, *Nature*, *445*, 908–911.

McCorkle, D. C., B. H. Corliss, and C. A. Farnham (1997), Vertical distribution and stable isotopic compostition of live (stained) benthic foraminifera from the North Carolina and California margins, *Deep Sea Res. Part I*, *44*, 983–1024.

Molina-Cruz, A., and M. Martinez-Lopez (1994), Oceanography of the Gulf of Tehuantepec, Mexico, indicated by Radiolaria remains, *Palaeogeogr. Palaeoclimatol. Palaeoecol.*, *110*, 179–195.

Muza, J. P., and W. W. J. Sherwood (1983), An authigenic gypsum, pyrite and glauconite association in a miocene deep-sea biogenic ooze from the Falkland plateau, Southwest Atlantic Ocean, *Initial Rep. Deep Sea Drill. Proj.*, *71*, 361–375.

Nöthen, K., and S. Kasten (2011), Reconstructing changes in seep activity by means of pore-water and solid-phase Sr/Ca and Mg/Ca ratios in pockmarks sediments of the Northern Congo Fan, *Mar. Geol.*, *287*, 1–13.

Paulmier, A., and D. Ruiz-Pino (2009), Oxygen Minimum Zones (OMZs) in the modern ocean, *Prog. Oceanogr.*, *80*, 113–128, doi:10.1016/j.pocean.2008.08.001.

Paytan, A., S. Mearon, K. Cobb, and M. Kastner (2002), Origin of marine barite deposits: Sr and S isotope characterization, *Geology*, *30*, 747–750.

Pearson, P. N., P. W. Ditchfield, J. Singano, K. G. Harcourt-Brown, C. J. Nicholas, R. K. Olsson, N. J. Shackleton, and M. A. Hall (2001), Warm tropical sea surface temperatures in the Late Cretaceous and Eocene epochs, *Science*, *413*, 481–487.

Peckmann, J., A. Reimer, U. Luth, C. Luth, B. T. Hansen, C. Heinicke, J. Hoefs, and J. Reitner (2001), Methane-derived carbonates and authigenic pyrite from the northwestern Black Sea, *Mar. Geol.*, *177*, 129–150.

Pfeifer, K., C. Hensen, M. Adler, F. Wenzhöfer, B. Weber, and H. D. Schulz (2002), Modeling of subsurface calcite dissolution, including the respiration and reoxidation processes of marine sediments, in the region of equatorial upwelling off Gabon, *Geochim. Cosmochim. Acta*, *66*, 4247–4259.

Pichevin, L. E., R. S. Ganeshram, S. Francavilla, E. Arellano-Torres, T. F. Pedersen, and L. Beaufort (2010), Interhemispheric leakage of isotopically heavy nitrate in the eastern tropical Pacific during the last glacial period, *Paleoceanography*, *25*, PA1204, doi:10.1029/2009PA001754.

Rees, C. E., W. J. Jenkins, and J. Monster (1978), The sulphur isotopic composition of ocean water sulphate, *Geochim. Cosmochim. Acta*, *42*, 377–381.

Reimers, C. E., K. C. Ruttenberg, D. E. Canfield, M. B. Christiansen, and J. B. Martin (1996), Porewater pH and authigenic phases formed in the uppermost sediments of the Santa Barbara Basin, *Geochim. Cosmochim. Acta*, *60*, 4037–4057.

Reuning, L., J. J. G. Reijmer, C. Betzler, P. Swart, and T. Bauch (2005), The use of paleoceanographic proxies in carbonate periplatform settings-opportunities and pitfalls, *Sediment. Geol.*, *175*, 131–152.

Riedinger, N., S. Kasten, J. Gröger, C. Franke, and K. Pfeifer (2006), Active and buried barite fronts in sediments from the Eastern Cape Basin, *Earth Planet. Sci. Lett.*, *241*, 876–887.

Riedinger, N., B. Brunner, M. J. Formolo, E. Solomon, S. Kasten, M. Strasser, and T. Ferdelman (2010), Oxidative sulfur cycling in the deep biospere of the Nankai Trough, Japan, *Geology*, *38*, 851–854.

Schippers, A., and B. B. Jørgensen (2001), Oxidation of pyrite and iron sulfide by manganese dioxide in marine sediments, *Geochim. Cosmochim. Acta*, *65*, 915–922, doi:10.1016/S0016-7037(00)00589-5.

Schlitzer, R. (2008), Ocean Data View, software, Alfred Wegener Inst., Bremerhaven, Germany. [Available at http://odv.awi.de.]

Schnitker, D., L. M. Mayer, and S. Norton (1980), Loss of calcareous microfossils from sediments through gypsum formation, *Mar. Geol.*, *36*, M35–M44.

Self-Trail, J. M., and E. L. Seefelt (2005), Rapid dissolution of calcareous nannofossils: A case study from freshly cored sediments of the South-Eastern Atlantic coastal plain, *J. Nannoplankton Res.*, *27*, 149–157.

Shackleton, N. J. (1974), Attainment of isotopic equilibrium between ocean water and the benthonic foraminifera genus Uvigerina: Isotopic changes in the ocean since the last glacial, in *Colloq. Int. C. N. R. S.*, *219*, pp. 203–209.

Siesser, W. G., and J. Rogers (1976), Authigenic pyrite and gypsum in South West African continental slope sediments, *Sedimentology*, *23*, 567–577.

Sperling, M., S. Welbeab, and G. Schmiedl (2002), Drying of samples may alter foraminiferal isotopic ratios and faunistic composition, *Micropaleontology*, *48*, 87–91.

Spero, H. J., K. M. Mielke, E. M. Kalva, D. W. Lea, and D. K. Pak (2003), Multispecies approach to reconstructing Eastern Equatorial Pacific thermocline hydrography during the past 360 kyr, *Paleoceanography*, *18*(1), 1022, doi:10.1029/2002PA000814.

Stott, L. D., T. Bunn, M. Prokopenko, C. Mahn, J. Gieskes, and J. M. Bernhard (2002), Does the oxidation of methane leave an isotopic fingerprint in the geologic record?, *Geochem. Geophys. Geosyst.*, *3*(2), 1012, doi:10.1029/2001GC000196.

Stuiver, M., P. J. Reimer, and R. Reimer (2005), Calib 5.0., software, Univ. of Wash., Seattle.

Thamdrup, B., H. Fossing, and B. Jorgensen (1994), Manganese, iron and sulfur cycling in a coastal marine sediment, Aarhus Bay, Denmark, *Geochim. Cosmochim. Acta*, *58*, 5115–5129, doi:10.1016/0016-7037(94)90298-4.

Thunell, R. C., W. B. Curry, and S. Honjo (1983), Seasonal variations in the flux of planktonic foraminifera: Time series sediment trap results from the Panama Bassin, *Earth Planet. Sci. Lett.*, *64*, 44–55.

Torres, M. E., H. J. Brumsack, G. Bohrmann, and K. C. Emeis (1996), Barite fronts in continental margin sediments: A new look at barium remobilization in the zone of sulfate reduction and formation of heavy barites in diagenetic fronts, *Chem. Geol.*, *127*, 125–139.

Torres, M. E., A. C. Mix, K. Kinports, B. Haley, G. P. Klinkhammer, J. McManus, and M. A. de Angelis (2003), Is methane venting at the seafloor recorded by δ^{13}c of benthic foraminifera shells?, *Paleoceanography*, *18*(3), 1062, doi:10.1029/2002PA000824.

Treude, T., J. Niggemann, J. Kallmeyer, P. Wintersteller, C. J. Schubert, A. Boetius, and B. B. Jørgensen (2005), Anaerobic oxidation of methane and sulfate reduction along the Chilean continental margin, *Geochim. Cosmochim. Acta*, *11*, 2767–2779.

Ussler, W., and C. K. Paull (1995), Effects of ion exclusion and isotopic fractionation on pore water geochemistry during gas hydrate formation and decomposition, *Geo Mar. Lett.*, *15*, 37–44.

van Geen, A., Y. Zheng, J. M. Bernhard, K. G. Cannariato, J. Carriquiry, W. E. Dean, B. W. Eakins, J. D. Ortiz, and J. Pike (2003), On the preservation of laminated sediments along the western margin of North America, *Paleoceanography*, *18*(4), 1098, doi:10.1029/2003PA000911.

Volbers, A. N. A., and R. Henrich (2002), Present water mass calcium carbonate corrosiveness in the eastern South Atlantic inferred from ultrastructural breakdown of *Globigerina bulloides* in surface sediments, *Mar. Geol.*, *186*, 471–1486.

Walbroeck, C., J. Labeyrie, E. Michel, J.-C. Duplessy, J. McManus, K. Lambeck, E. Balbon, and M. Labracherie (2002), Sea-level and deep water temperature changes derived from benthic foraminifera isotopic record, *Quat. Sci. Rev.*, *21*, 295–305.

Werne, J. P., T. W. Lyons, D. J. Hollander, S. Schouten, E. C. Hopmans, and J. Sinninghe Damsté (2008), Investigating pathways of diagenetic organic matter sulfurization using compound-specific sulfur isotope analysis, *Geochim. Cosmochim. Acta*, *72*, 3489–3502.